

CFD modeling of the high-temperature HVPE growth of aluminum nitride layers on *c*-plane sapphire: from theoretical chemistry to process evaluation

R. Boichot · N. Coudurier · F. Mercier ·
A. Claudel · N. Baccar · A. Milet · E. Blanquet ·
M. Pons

Received: 28 June 2013 / Accepted: 4 November 2013 / Published online: 29 November 2013
© Springer-Verlag Berlin Heidelberg 2013

Abstract This study presents numerical modeling based on a relatively limited number of gas-phase and surface reactions to simulate the growth rate of aluminum nitride layers on AlN templates and *c*-plane sapphire in a broad range of deposition parameters. Modeling results have been used to design particular experiments in order to understand the influence of the process parameters on the crystal quality of AlN layers grown in a high-temperature hydride vapor-phase epitaxy process fed with NH₃, AlCl₃, and H₂. Modeling results allow to access to very interesting local quantities such as the surface site ratio and local supersaturation. The developed universal model starting from local parameters might be easily transferred to other reactor geometry and process conditions. Among the investigated parameters (growth rate, temperature, local supersaturation, gas-phase N/Al ratio, and local surface site N/Al ratio), only the growth rate/supersaturation or growth rate/

temperature relationships exhibit a clear process window to use in order to succeed in growing epitaxial AlN layers on *c*-plane sapphire or AlN templates. Gas-phase N/Al ratio and local surface site N/Al ratio seem to play only a secondary role in AlN epitaxial growth.

Keywords AlN · High-temperature HVPE · Numerical modeling · Epitaxial growth

List of symbols

| | |
|-----------------------|--|
| (S) | Surface site |
| (B) | Bulk or solid species |
| $[A]$ | Gas-phase concentration of species A (mol m^{-3}) |
| a_k | Pre-exponential factor for reaction k (consistent units) |
| $[C(S)]$ | Surface site concentration of species C (mol m^{-2}) |
| E_{ak} | Activation energy for reaction k (J mol^{-1}) |
| k_k | Rate constant for reaction k (s^{-1} or $\text{mol}^{-1} \text{m}^3 \text{s}$ or $\text{mol}^{-2} \text{m}^6 \text{s}$) |
| M | Unspecified species (–) |
| M_A | Molar mass for gaseous specie A (kg mol^{-1}) |
| P_A | Partial pressure of A at the growing AlN surface (Pa) |
| P_A^* | Equilibrium pressure of A versus AlN in vacuum (Pa) |
| R | Ideal gas constant ($\text{J mol}^{-1} \text{K}^{-1}$) |
| T | Temperature (K) |
| β_k | Temperature exponent for reaction k (–) |
| γ_A | Sticking coefficient for gaseous species A (–) |
| γ_0 | Pre-exponential factor for the sticking coefficient (–) |
| Γ_{tot} | Total surface site concentration (mol m^{-2}) |
| v_k | Production rate of solid surface for reaction k ($\text{mol m}^{-2} \text{s}^{-1}$) |

Published as part of a special collection of articles focusing on chemical vapor deposition and atomic layer deposition.

R. Boichot (✉) · N. Coudurier · F. Mercier · N. Baccar ·
E. Blanquet · M. Pons
SIMaP CNRS, Grenoble INP, UJF, 1130 Rue de la Piscine,
38402 Saint Martin d'Hères, France
e-mail: raphael.boichot@simap.grenoble-inp.fr

N. Coudurier · A. Claudel
ACERDE, 354 Voie Magellan, AlpeSPACE,
73800 Ste Hélène du Lac, France

A. Milet
DCM Chimie Théorique, Bâtiment Chimie C,
38402 Saint Martin d'Hères, France

1 Introduction

Aluminum nitride is a promising substrate for AlGaN-based UV LED (intended to be used for water purification and optical information storage) and piezoelectric applications [micro-electro-mechanical systems (MEMS) and surface acoustic waves (SAW) devices]. The UV LED industry requires high-quality single crystals (i.e., deep UV transparency, low density of defect) [1]. The requirements are more accessible for piezoelectric applications, for which crack-free highly oriented *c*-axis layers are needed [2, 3]. Heteroepitaxy is necessary for the development of these new devices and systems, due to the fact that it is currently the cheapest solution to produce industrial grade AlN single crystals. Among the different available processes for AlN growth (physical vapor transport, PVT [4], metal-organic chemical vapor deposition, MOCVD [5], and high-temperature hydride vapor-phase epitaxy (HT-HVPE) [6–16]), high-temperature HVPE (>1,200 °C) becomes the most prospective technique to produce the required quality for both piezoelectric and semiconductor industry. Despite its considerable interest, this technique is still little studied from a modeling point of view. A better understanding of the phenomena leading to high-quality AlN layers grown on sapphire is the key point to allow high-temperature HVPE becoming a new industrial reference in thick AlN layers processing.

High-temperature CVD processes are commonly used to produce thick layers of AlN on various substrates. The halide process using Al chloride and NH₃ or N₂ as Al and N-precursors, respectively, is the most commonly used. The experimental and thermodynamic study of Nickel et al. [6] very early assessed the possibility to fabricate AlN layers from AlCl₃ and NH₃ precursors. Attempts to obtain epitaxial growth on sapphire are more recent one. Kumagai et al. [7, 8], Freitas et al. [9], Nagashima et al. [10], Eriguchi et al. [11, 12], and Tajima et al. [13] succeeded in growing AlN on (0001) sapphire substrates in a hot-wall reactor, in the 900–1,550 °C temperature range. Claudel et al. [14–16] obtained similar results in a cold-wall reactor.

Kinetic mechanisms of AlN deposition from chlorinated precursors were first initiated by Allendorf's team [17–20]. They proposed a set of kinetic and thermodynamic data for the B–Cl–N–H system, complemented by the reaction set of NH₃ pyrolysis [21]. Dollet et al. [22] extrapolated the gas-phase kinetic data for AlN formation from the work of these previous authors and proposed sticking coefficients for AlCl₃ and NH₃ on a growing AlN surface. Their study reported a mechanism where AlCl₃ and AlCl₂NH₂ are the main aluminum containing species precursors. However, only irreversible gas-phase reactions for the formation of AlCl₂NH₂ were used due to a lack of available

thermodynamic data for this species. At the same time, Swihart et al. [23] proposed a comprehensive kinetic data set for the Al–Cl–H system from ab initio calculations.

Recently, Cai et al. [24, 25] proposed from the data of [22] an irreversible gas-phase growth mechanism involving AlCl₃, AlCl₂NH₂, AlCl(NH₂)₂, Al(NH₂)₃, and AlClNH, as aluminum containing species, neglecting the surface kinetic of NH₃ absorption (NH₃ in large excess), and using the pre-exponential factors of Arrhenius laws as fitting parameters. Segal et al. [26] similarly conducted a mass transport and quasi-thermodynamic surface kinetic model for AlN growth.

We have also previously developed [27] and proposed a complete description of heat transfer, mass transport, gas flow dynamics and chemical reactions based on available data [21–23] and experimental data of AlN growth on AlN templates. This modeling work [27] included a complete thermodynamic modeling of the species involved in the database reported in Ref. [22] and proposed forward and backward reactions rates in the Al–Cl–N–H system. The fitting between experimental and numerical results was made via the activation energy of the surface reactions.

The aim of the present study is (1) to extend previous modeling results with the help of new experiments covering a broader range of experimental parameters (temperature from 900 to 1,500 °C, N/Al ratio in gas phase from 0.75 to 30, total pressure fixed at 1,333 Pa, partial pressure of precursors of Al- and N-containing reactive species from 0.5 to 120 Pa) and (2) to increase the understanding of the effect of both N/Al ratio and supersaturation in the gas phase on the crystalline quality of AlN layers grown on sapphire.

2 Numerical modeling

2.1 Model formalism: gas-phase kinetic and equilibrium analysis

All the calculations presented in this paper were performed using the CFD-ACE multiphysics software package (2012 v1—<http://www.esi-group.com>), using the geometry of the vertical and axisymmetric reactor described in Ref. [27].

In the high-temperature HVPE process used in this study, NH₃ was used as nitrogen source, Al chloride (mainly AlCl₃) fabricated from Al in situ chlorination as aluminum source, and H₂ as carrier/reactive gas. In consequence, an exhaustive study of the Al–Cl–N–H system has been conducted in order to highlight particular kinetic pathways.

Thermodynamic and kinetic analysis presented in Ref. [27] leads to the following simplified set of elementary gas-

Table 1 Gas-phase reaction kinetic parameters

| Reaction | a_k | β_k | E_{ak}/R | a_k | β_k | E_{ak}/R |
|---|-----------------|------------|------------------|---|------------|------------------|
| | Pre exp. factor | Temp. exp. | Activ. temp. (K) | Pre exp. factor | Temp. exp. | Activ. temp. (K) |
| | Forward rates | | | Backward rates | | |
| $\text{AlCl}_3 + \text{NH}_3 \leftrightarrow \text{AlCl}_2\text{NH}_2 + \text{HCl}$ | 4.21E+05 | 0 | 4,198 | Calculated by thermodynamic equilibrium | | |
| $\text{H}^\circ + \text{Cl}^\circ + \text{M} \leftrightarrow \text{HCl} + \text{M}$ | 7.20E+09 | -2 | 0 | 7.90E+19 | -3 | 53,598 |
| $2\text{Cl}^\circ + \text{M} \leftrightarrow \text{Cl}_2 + \text{M}$ | 2.00E+02 | 0 | -901 | Calculated by thermodynamic equilibrium | | |
| $\text{H}^\circ + \text{HCl} \leftrightarrow \text{Cl}^\circ + \text{H}_2$ | 1.69E+07 | 0 | 2,082 | 2.95E+07 | 0 | 2,567 |
| $\text{Cl}_2 + \text{H}^\circ \leftrightarrow \text{Cl}^\circ + \text{HCl}$ | 8.60E+07 | 0 | 590 | Calculated by thermodynamic equilibrium | | |
| $2\text{H}^\circ + \text{H}_2 \leftrightarrow 2\text{H}_2$ | 9.70E+04 | -0.6 | 0 | 8.80E+08 | 0 | 48,364 |
| $\text{H}_2 + \text{M} \leftrightarrow 2\text{H}^\circ + \text{M}$ | 2.20E+08 | 0 | 48,364 | 6.53E+5 | -1 | 0 |

Units are given in K s mol m. M is an unspecified third-body species

phase reactions as relevant to model the AlN growth rate. The rate constant for each reaction is expressed in the form of a classical Arrhenius law (for reaction k):

$$k_k = a_k T^{\beta_k} \exp\left(\frac{-E_{ak}}{RT}\right). \quad (1)$$

Table 1 gives the kinetic parameters for each elementary gas-phase reaction (the order with respect to each reactant is 1).

Reactions in H–Cl system of Table 1 are optional and are only needed to increase the precision of the mass transport modeling (see Table 2 also). For unknown backward rates, the equilibrium constant is calculated according to Ref. [28].

2.2 Mass transport modeling and surface reactions

The species transport properties are evaluated by various methods. The diffusion coefficients, mixtures viscosities, and mixtures thermal conductivities are calculated using the Enskog theory [29]. The Lennard–Jones parameters used for each gaseous species are either taken in the data reported in Refs. [29, 30] or computed according to the empirical method presented in Ref. [30]. The transport equations for gas species do not take into account the multi-component Stephan Maxwell formalism, due to the low concentration of reactive species in H_2 [29, 31]. Since the Reynolds number in our CVD reactor never exceeds 50, the laminar incompressible Navier–Stokes equation is solved to obtain the convective part of the diffusion-convection problem. The local density of fluid follows an ideal gas law.

To compute the mixture enthalpy, the JANAF formalism [32] is used. Each thermal property (i.e., entropy, enthalpy, and heat capacity) is calculated by a polynomial relationship with temperature. The used polynomial coefficients are taken from the Sandia National Laboratory Database [33].

For surface reactions, the atomic site formalism proposed in Ref. [34] is adopted. It is considered that each site is an atom chemically bonded to the surface. Two kinds of atomic sites (atoms) are available on growing AlN surfaces: Al(S) and N(S) sites. The total number of sites is initially evaluated as the atom surface concentration on the polar c -plane of the AlN wurtzite polytype ($1.98 \times 10^{-5} \text{ mol m}^{-2}$). The surface reaction rate for gas-phase molecules A approaching complementary atomic sites $C(S)$ is expressed as [34]:

$$v_k = k_k [A] \times [C(S)] \quad \text{with} \quad k_k = \sqrt{\frac{RT}{2\pi M_A}} \frac{\gamma_A}{[\Gamma_{\text{tot}}]}. \quad (2)$$

The ratio $C(S)/[\Gamma_{\text{tot}}]$ represents the fraction of surface sites C available for the sticking of gas-phase A molecules. The surface production rate is simply expressed as the product of an atom flux (kinetic theory of gases) with a probability that an atom of this flux sticks on the solid surface. We choose to express a simple dependency of the sticking coefficient γ_A with temperature:

$$\gamma_A = \gamma_0 \exp\left(\frac{-E_{ak}}{RT}\right). \quad (3)$$

In Eq. (3), $\gamma_0 = 1$ is taken as simplifying assumption. The activation temperatures for each surface reaction were varied in order to minimize the relative difference between computed and experimental AlN growth rates (results presented in the next section). In order to fit the rate constant k_k for surface reaction to the Arrhenius law of Eq. (1), the following changes of variables is used as follows:

$$\begin{aligned} a_k &= \sqrt{\frac{R}{2\pi M_A}} \frac{1}{[\Gamma_{\text{tot}}]} \\ \beta_k &= 0.5 \\ \frac{E_{ak}}{R} \Big|_{\text{Surface Arrhenius law}} &= \frac{E_{ak}}{R} \Big|_{\text{Sticking coefficient}} \end{aligned} \quad (4)$$

Table 2 Optimized surface kinetic parameters for AlN growth

| Surface reactions Reaction | a_k Pre exp. factor | β_k Temp. exp. | E_{ak}/R Activ. temp (K) |
|--|--------------------------|-------------------------|-------------------------------|
| $\text{NH}_3 + \text{Al}(S) \leftrightarrow \text{N}(S) + \text{H}_2 + \text{H}^\circ$ | 4.453E+05 | 0.5 | 8,654 |
| $\text{AlCl}_3 + \text{N}(S) \leftrightarrow \text{AlN}(B) + \text{Al}(S) + \text{Cl}^\circ + \text{Cl}_2$ | 1.590E+05 | 0.5 | 7,700 |
| $\text{AlCl}_2\text{NH}_2 + \text{Al}(S) \leftrightarrow \text{AlN}(B) + \text{Al}(S) + 2\text{HCl}$ | 1.720E+05 | 0.5 | 5,100 |
| $\text{AlCl}_2\text{NH}_2 + \text{N}(S) \leftrightarrow \text{AlN}(B) + \text{N}(S) + 2\text{HCl}$ | 1.720E+05 | 0.5 | 5,100 |

Units are given in K s mol m. Data corrected from Ref. [27]

This form is mandatory to enter the surface kinetics into CFD-ACE multiphysics software database. Table 2 gives the kinetic parameters for each elementary surface reaction, according to this change of variables (the order with respect to each reactant is 1). The surface reactions are considered irreversible (no etching taken into account).

It should be noticed that the experimental activation temperature for AlN growth is about 7,460 K (62 kJ mole⁻¹) and that the transition between kinetic-limited growth and diffusion-limited growth is observed from 1,200 to 1,300 °C. The modeling presented here covers both diffusion and kinetic regime.

Solving numerically the balance of chemical site on the AlN surface gives access to the surface N(S)-Al(S) ratio during growth. This balance is simply obtained by assuming that the molar rate of absorption of nitrogen and aluminum atoms is the same (growth of stoichiometric ⟨AlN⟩). Then, the site density in Eq. (3) is calculated in order to satisfy this equality. This balance is performed by the CFD-ACE multiphysics software during calculations.

The validity of the modeling already presented in Ref. [27] will be confronted to new experimental data. The numerical modeling will give an accurate estimation of growth rates, but will also allow calculating the surface site ratio N(S)-Al(S) on AlN and estimating the surface supersaturation of gaseous species in front of the growing AlN surface. Indeed, the surface partial pressure of precursors strongly differs from the inlet partial pressure in diffusion-limited regime. These local site ratios and supersaturations will be confronted to the AlN crystal quality to evaluate if there is an apparent correlation.

General trends on the correlation between calculated gas-phase supersaturation and morphology of CVD films have already been reported in Ref. [35]. It is generally accepted that with increasing supersaturation, the sequence obtained for the morphology is epitaxial layer, whiskers, polycrystallites, amorphous layer, and finally homogeneous nucleation.

Several authors have defined supersaturation in the past [36–41], with different forms within a general concept that represents the difference in thermodynamic potential between the initial and the final equilibrium states. The sum or product of the reactants pressure divided by the sum or product of the species pressure at equilibrium can be

used in equations. The sum presents the obvious property of being nondimensional whatever the number of species taken into account in each side of the division. In the frame of our study, the local gas supersaturation near the growing surface has been defined as follows:

$$\beta = \frac{P_{\text{AlCl}_3} + P_{\text{NH}_3} + 2P_{\text{AlCl}_2\text{NH}_2}}{P_{\text{Al}}^* + 2P_{\text{N}_2}^*} \quad (5)$$

where P is the calculated pressure of species contributing to AlN growth just in front of the growing surface and P^* the equilibrium vapor pressure of gases (N₂ and Al) in equilibrium with ⟨AlN⟩ in a closed volume, at the same temperature, without hydrogen. As ⟨AlN⟩ becomes theoretically unstable in hydrogen between 1,200 and 1,300 °C [27], the “AlN vapor pressure” in H₂ has no meaning (i.e., the supersaturation is equal to unity in the range 1,200–1,600 °C). This confirms that the growth conditions are far from thermodynamic equilibrium inasmuch as AlN growth is observed in conditions where ⟨AlN⟩ is theoretically unstable (under H₂ for HT-HVPE). The values P^* are calculated with Factsage 6.0 software package, with the SGTE database [42].

All the calculations performed here have been conducted with updated databases for transport, thermodynamic, and kinetic properties. In consequence, the modeling results related to the experimental data of Ref. [27] may be slightly different from the modeling results presented here.

2.3 Experiments

Experiments were carried out in a vertical tubular quartz cold-wall HTCVD reactor depicted in Ref. [27]. AlCl₃ is produced in situ by direct chlorination of high-purity aluminum pellets (99.9999 %) under a Cl₂ flux at 640 °C [14]. The aluminum precursor is then mixed with NH₃ previously diluted in a large amount of H₂ as carrier and reactive gas. The total pressure is 1,333 Pa. Quarters of two-inch-diameter *c*-plane (±0.1°) sapphire wafers are used as substrates. Prior to the injection of reactive gases, both aluminum pellets and substrate are slowly heated under H₂. A 10-min annealing under H₂ at 1,100 °C is used to prepare the sapphire surface (etching of carbon contaminants); then, the ramp-up to the growing temperature is made

Table 3 Summary of the growth parameters

| Temperature (°C) | N/Al ratio in gas phase | Secm NH ₃ | Secm Cl ₂ | Deposit duration (min) | Measured thickness (μm) | Measured growth rate (μm h ⁻¹) | Theoretical growth rate (μm h ⁻¹) | Log10 surface sursaturation | Surface N(S)/Al(S) | Crystal quality | FWHM (0002) (arc) sec | Comment | Substrate |
|------------------|-------------------------|----------------------|----------------------|------------------------|-------------------------|--|---|-----------------------------|--------------------|-----------------|-----------------------|-------------------------|-------------------------------|
| 900 | 4.5 | 30 | 10 | 60 | 5 | 5.0 | 6.8 | 6.688 | 6.62 | Polycrystal | – | Calibration experiments | AlN template/c-plane sapphire |
| 1,150 | 4.5 | 30 | 10 | 60 | 15 | 15.0 | 14.9 | 3.401 | 9.31 | Polycrystal | – | Calibration experiments | AlN template/c-plane sapphire |
| 1,300 | 4.5 | 30 | 10 | 60 | 25 | 25.0 | 20.0 | 1.931 | 11.50 | Polycrystal | – | Calibration experiments | AlN template/c-plane sapphire |
| 1,500 | 4.5 | 30 | 10 | 60 | 35 | 35.0 | 25.8 | 0.360 | 15.09 | Polycrystal | – | Calibration experiments | AlN template/c-plane sapphire |
| 1,400 | 30 | 100 | 5 | 60 | 14 | 14.0 | 14.1 | 1.593 | 155.20 | Polycrystal | – | Calibration experiments | AlN template/c-plane sapphire |
| 1,400 | 1.5 | 50 | 5 | 60 | 12 | 12.0 | 134 | 1.312 | 59.35 | Polycrystal | – | Calibration experiments | AlN template/c-plane sapphire |
| 1,400 | 6 | 20 | 5 | 60 | 10 | 10.0 | 11.7 | 0.929 | 18.23 | Polycrystal | – | Calibration experiments | AlN template/c-plane sapphire |
| 1,400 | 4.5 | 15 | 5 | 60 | 14 | 14.0 | 11.2 | 0.809 | 12.63 | Polycrystal | – | Calibration experiments | AlN template/c-plane sapphire |
| 1,400 | 1.5 | 5 | 5 | 60 | 10 | 10.0 | 9.1 | 0.381 | 2.83 | Epitaxial | 3,204 | Calibration experiments | AlN template/c-plane sapphire |
| 1,400 | 0.75 | 21 | 42 | 5 | 10 | 120.0 | 60.8 | 1.106 | 0.97 | Polycrystal | – | Constant sursaturation | c-plane sapphire |
| 1,400 | 1.5 | 29.4 | 29.4 | 7.5 | 10 | 80.0 | 56.2 | 1.122 | 2.93 | Polycrystal | – | Constant sursaturation | c-plane sapphire |

Table 3 continued

| Temperature (°C) | N/Al ratio in gas phase | Scm NH ₃ | Scm Cl ₂ | Deposit duration (min) | Measured thickness (μm) | Measured growth rate (μm h ⁻¹) | Theoretical growth rate (μm h ⁻¹) | Log10 surface sursaturation | Surface N(S)/Al(S) | Crystal quality | FWHM (0002) (arc) sec | Comment | Substrate |
|------------------|-------------------------|---------------------|---------------------|------------------------|-------------------------|--|---|-----------------------------|--------------------|-----------------|-----------------------|-------------------------------------|------------------|
| 1,400 | 3 | 36.75 | 18.4 | 14 | 17 | 72.9 | 40.5 | 1.184 | 7.91 | Polycrystal | – | Constant sursaturation | c-plane sapphire |
| 1,400 | 6 | 42 | 10.5 | 21 | 10 | 28.6 | 25.2 | 1.236 | 19.35 | Polycrystal | – | Constant sursaturation | c-plane sapphire |
| 1,400 | 9 | 44.1 | 7.3 | 33 | 10 | 18.2 | 18.4 | 1.258 | 31.73 | Polycrystal | – | Constant sursaturation | c-plane sapphire |
| 1,300 | 3 | 5.2 | 2.6 | 60 | 7.5 | 7.5 | 5.4 | 1.185 | 7.30 | Polycrystal | – | Constant sursaturation | c-plane sapphire |
| 1,450 | 3 | 88 | 44 | 15 | 32 | 128.0 | 95.4 | 1.158 | 8.25 | Polycrystal | – | Constant sursaturation | c-plane sapphire |
| 1,500 | 0.75 | 2.2 | 4.44 | 75 | 8.05 | 6.4 | 7.0 | -0.604 | 0.93 | Epitaxial | 5,011 | Constant thickness and growth rates | c-plane sapphire |
| 1,500 | 1.5 | 3.5 | 3.5 | 75 | 7.90 | 6.3 | 7.3 | -0.528 | 3.04 | Epitaxial | 1,418 | Constant thickness and growth rates | c-plane sapphire |
| 1,500 | 3 | 6.1 | 3.05 | 75 | 5.86 | 4.7 | 7.2 | -0.311 | 8.26 | Epitaxial | 3,888 | Constant thickness and growth rates | c-plane sapphire |
| 1,500 | 7.5 | 13.9 | 2.78 | 75 | 5.36 | 4.3 | 7.2 | 0.042 | 26.47 | Epitaxial | 3,222 | Constant thickness and growth rates | c-plane sapphire |
| 1,500 | 15 | 27.5 | 2.75 | 75 | 7.01 | 5.7 | 7.8 | 0.333 | 64.04 | Epitaxial | 950 | Constant thickness and growth rates | c-plane sapphire |
| 1,500 | 30 | 52.5 | 2.62 | 75 | 4.54 | 3.6 | 8.0 | 0.606 | 162.30 | Epitaxial | 3,528 | Constant thickness and growth rates | c-plane sapphire |
| 1,200 | 3 | 3 | 1.5 | 10 | 0.17 | 1.0 | 24 | 1.919 | 5.70 | Epitaxial | 403 | Protective layer | c-plane sapphire |
| 1,500 | 1.5 | 3.5 | 3.5 | 75 | 4.03 | 3.2 | 7.3 | -0.528 | 3.04 | Epitaxial | 327 | Two steps growth | c-plane sapphire |

Pressure is 1,333 Pa and H₂ carrier gas flow rate of 1,000 sscm during deposition. Scm stands for “standard cubic centimeter per minute,” 1 sccm = 7.44×10^{-7} mol s⁻¹

under 0.02:NH₃/1:H₂ at 20 °C min⁻¹. At the growth temperature, chlorine is injected into the aluminum chloride generator and NH₃ is readily inserted into H₂. At the end of the experiment, Cl₂ flow is first stopped and then NH₃, and finally, the substrate is slowly cooled down under H₂ at 10 °C min⁻¹. The diluting gas flow rate during growth is systematically 1,000 sccm of H₂. AlN film thickness and surface morphology are measured and observed by scanning electron microscopy (SEM) or field emission gun (FEG)–SEM. The thicknesses are obtained by averaging 5–10 SEM thickness measurements at different locations of a cross section of the grown layer. The substrates are set on a graphite susceptor during experiments. It was observed that a N/Al ratio above 0.75 in the gas phase leads to a strong etching of the susceptor, releasing gaseous chlorine–carbon contaminants and thus limiting the lower value that can be explored for this parameter.

Table 3 summarizes the experiments performed for this study. The experimental growth rates, experimental conditions, calculated local supersaturations, calculated surface sites ratio, and crystal characteristics are given. The crystal quality is either polycrystalline (X-ray diffraction measurements in Bragg–Brentano configuration presenting many peaks related to different AlN orientations), or epitaxial (only (000n) AlN diffraction peaks). The FWHM (full width at half maximum) of the (0002) diffraction peak of XRD rocking curves is indicated as a criterion for crystalline quality of epitaxial AlN layers (wurtzite phase).

Every growth experiment has been conducted at least two times to ensure the repeatability. The thickness uncertainty is under 10 % of the total layer thickness.

Table 3 presents three distinct sets of experiments (see comments column of Table 3). The first set has been already presented and discussed in our previous study [27]. It was used to calibrate the numerical modeling of AlN growth. AlN templates were deliberately used to overcome heteroepitaxial issues with growth kinetics. Only one condition leads to AlN epitaxial growth on AlN template. It is obtained for the lowest supersaturation and N/Al ratio. Epitaxial growth cannot be attributed to one parameter or the other [27].

The second set of experiments has been designed with mass transport modeling in order to vary the N/Al ratio in gas phase at nearly constant surface supersaturation and for a constant layer thickness. Due to the high growth rates obtained, none of the experiments led to epitaxial growth.

Finally, the objective of the third set of experiments also designed by mass transport modeling was to assess the influence of N/Al ratio in gas phase at constant thickness and constant growth rate of the layer. More detailed results can be found in Ref. [43]. Additionally, in this set of experiments, the influence of a low-temperature protective layer prior the growth of thick high-temperature AlN layers is presented. All

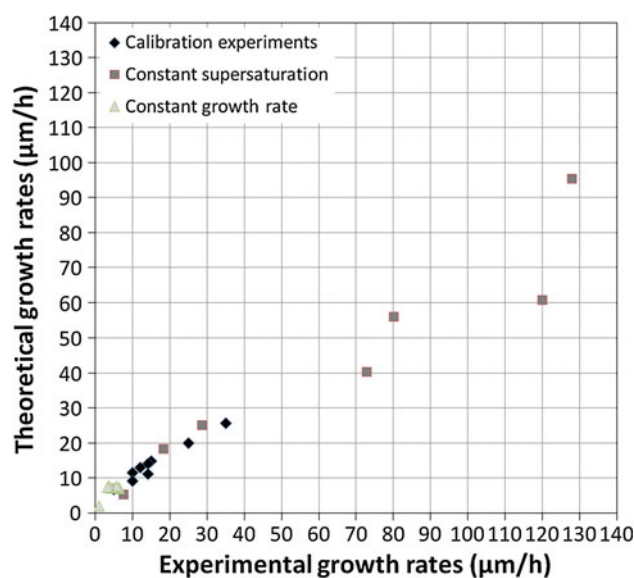


Fig. 1 Parity diagram between experimental and theoretical growth rates

the experiments led to epitaxial layers, with varying crystal qualities due to the presence of etching voids at the sapphire/AlN interface. These voids are suppressed by growing a low-temperature protective layer prior to the growth of the high-temperature thick AlN layer. The growth is then divided into two steps: a low-temperature step that leads to the deposition of an AlN protective layer and a high-temperature step that leads to the deposition of the thick AlN layer. The process flowcharts can be found in Ref. [43]. Both the low-temperature protective layer and the high-temperature layer step are described in Table 3 (two last lines).

The calculated supersaturation can reach values below 1 [$\text{Log}_{10}(\beta) < 0$] due to the fact that theoretical equilibrium partial pressure of AlN ($\text{Al} + 1/2\text{N}_2$) on solid $\langle\text{AlN}\rangle$ is greater than the partial pressure of reactants. The supersaturation values can be at least compared between each other.

The following discussion presents a local analysis of the major quantities at the growth front that influence or not the AlN crystal characteristics.

3 Results and discussion

3.1 Experimental growth rates versus modeling

First, the overall parity diagram between simulated and experimental growth rates is presented in Fig. 1.

The optimization of surface kinetic parameters has been made by minimizing the relative difference between experimental and simulated growth rate, with a limited number of parameters (only the three activation temperatures for sticking coefficients). The modeling results

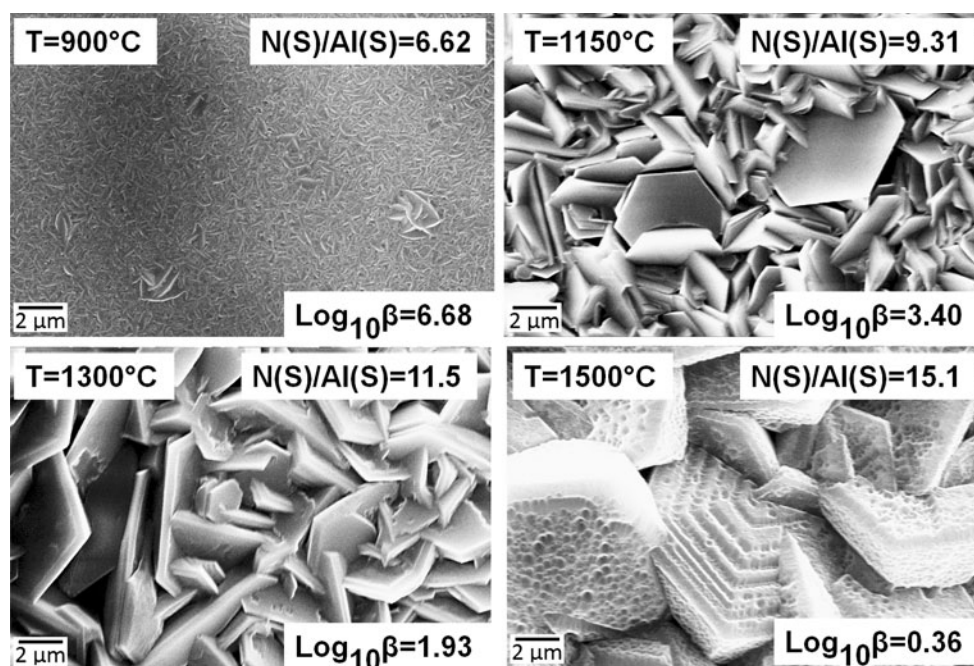


Fig. 2 Surface morphology at different temperatures for $N/Al = 4.5$ in the gas phase (calibration experiment set on AlN template). The figure also indicates the surface $N(S)/Al(S)$ ratio and the local $\text{Log}_{10}\beta$ of the supersaturation

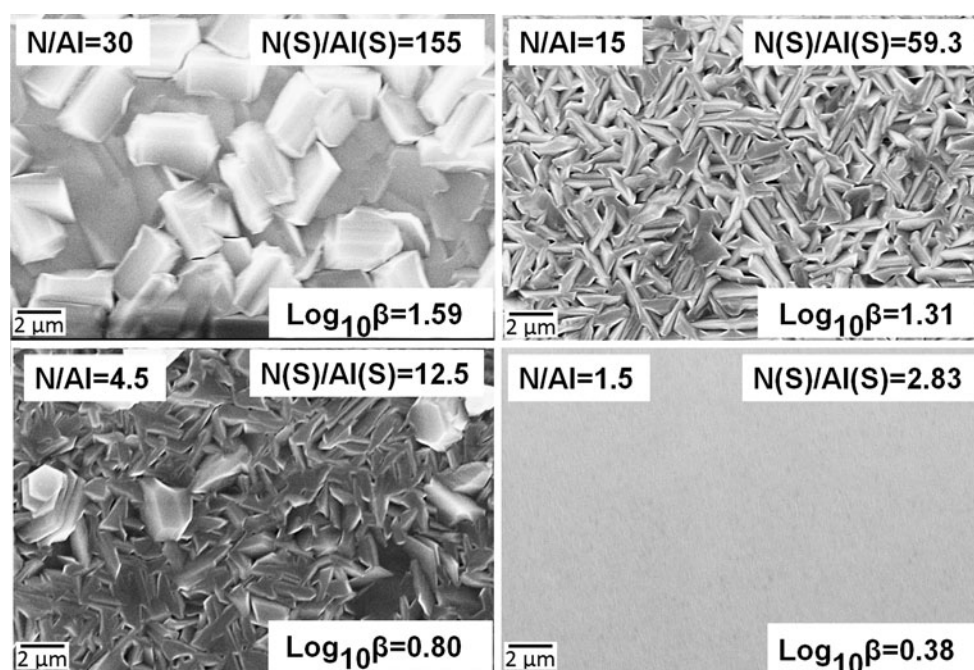


Fig. 3 Surface morphology for different N/Al ratio in the gas phase at constant temperature (calibration experiment set on AlN templates, $T = 1,400$ °C). The figure also indicates the surface $N(S)/Al(S)$ ratio and the local $\text{Log}_{10}\beta$ of the supersaturation

overestimate the lower growth rates and underestimate the higher growth rates. To obtain a better fitting, more calibration parameters could be used. But the model accurately predicts the influence of temperature and N/Al ratio in gas phase on the growth rate in a large range of experimental conditions in both kinetic and transport-limited regimes.

3.2 Morphology versus supersaturation and N/Al ratio

As stated in the Numerical Modeling section, the morphology is strongly influenced by the local supersaturation of reactive species. The effect of N/Al ratio both at the surface and in the gas phase is also important.

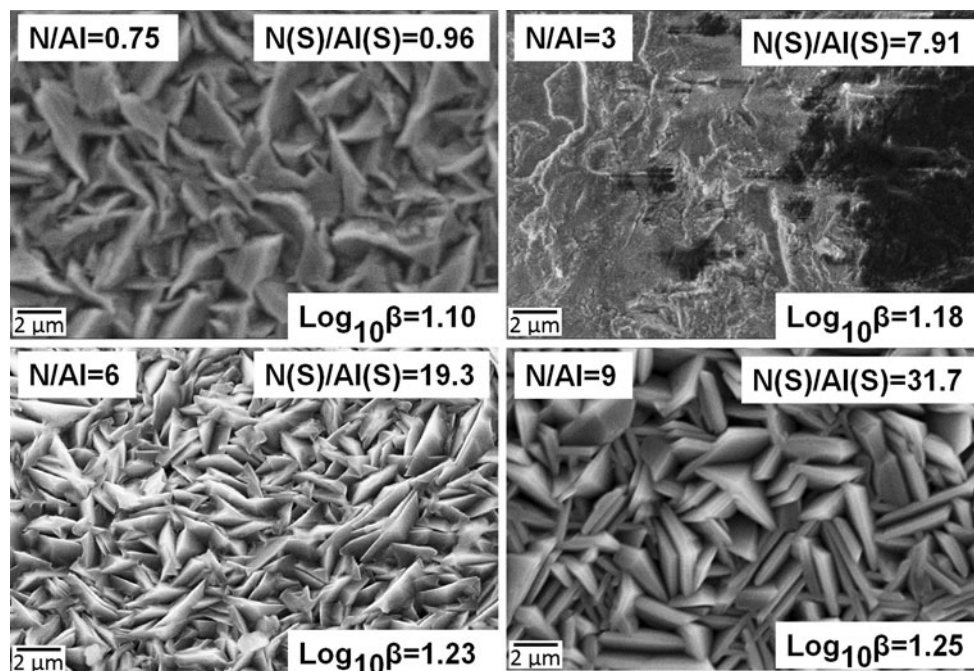


Fig. 4 Surface morphology for different N/Al ratio in the gas phase at constant supersaturation (constant supersaturation set, growth on sapphire, $T = 1,400$ °C). The figure also indicates the surface N(S)/Al(S) ratio, the gas-phase N/Al ratio, and the local Log_{10} of the supersaturation

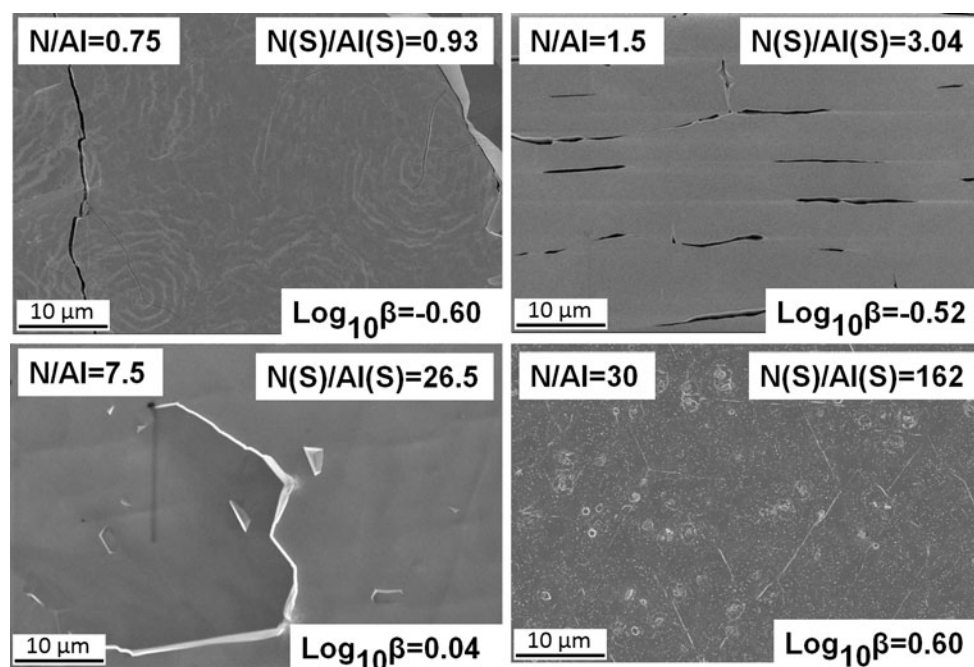


Fig. 5 Surface morphology for different N/Al ratio in the gas phase at constant growth rate and constant thickness (constant thickness and constant growth rate set, growth on sapphire, $T = 1,500$ °C). The figure also indicates the surface N(S)/Al(S) ratio and the local Log_{10} of the supersaturation

Typical SEM or FEG-SEM images of the surface morphologies of grown AlN layers with temperature, local supersaturation, gas-phase N/Al, and surface N(S)/Al(S) ratios indicated are given in Figs. 2, 3, 4, and 5.

Figure 2 shows, with larger grains on the surface morphology, the enhancement of adatoms surface diffusion coefficients with an increase in the temperature. In spite of lower supersaturation at high temperature, the experiment performed at 1,500 °C does not lead to epitaxial growth.

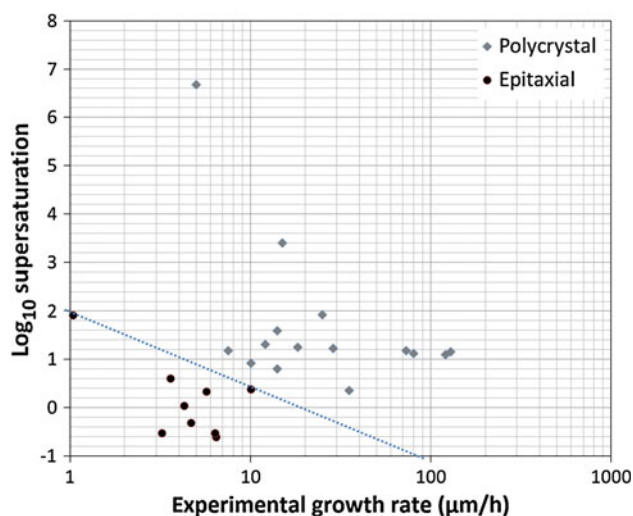


Fig. 8 Surface supersaturation versus experimental growth rate

of AlCl_3 , leading to a $N(S)/\text{Al}(S)$ close to 1. This trend is shown on Fig. 6.

According to Fig. 6, the rate limiting the AlN growth is the aluminum containing species kinetic (in HVPE conditions and according to our simplified kinetic scheme).

Consequently, $N(S)/\text{Al}(S)$ ratio and N/Al ratio are not independent parameters of our study. For sake of clarity, only the N/Al ratio in gas phase will be now presented.

Figure 7 presents a plot of the experimental growth rate versus the N/Al ratio in the gas phase for epitaxial and polycrystalline layers.

There is no clear correlation between epitaxial growth and N/Al ratio in the gas phase, but the AlN quality is clearly linked to the growth rate. However, at N/Al ratio of 1.5 in the gas phase, the process conditions leading to epitaxial growth seem to be broader in terms of range of growth rates. Clearly, the N/Al ratio parameter is not of prime interest for growing epitaxial AlN layers, but seems to play a role in the fine tuning of crystal quality. The optimum in crystal quality empirically observed at $N/\text{Al} = 1.5$ at $1,500^\circ\text{C}$ and 3 at $1,200^\circ\text{C}$ is not correlated to any particular local growing conditions. It could be emphasized that for these ratios, the surface diffusivity of absorbed species (not computed in our simple modeling) is related to the minimization of stacking faults during the AlN lattice growth.

Figure 8 represents the supersaturation versus the experimental growth rate for epitaxial and polycrystalline layers.

Figure 8 clearly allows defining of a process window where growing parameters lead to epitaxial growth of AlN on *c*-plane sapphire. This window ranges from relatively high supersaturation at low temperature, but very low growth rates to low supersaturation and growth rates as

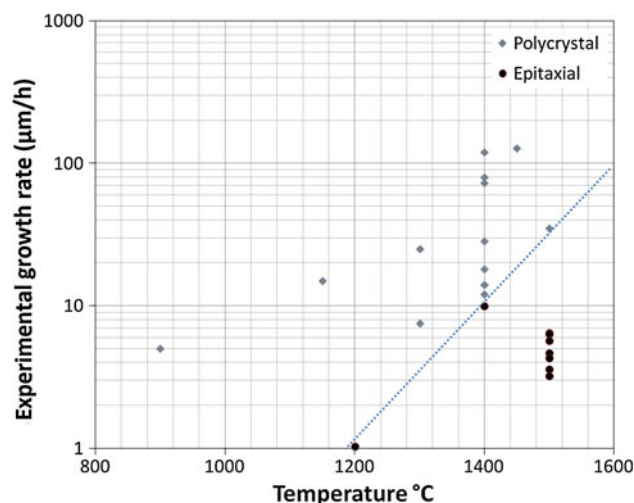


Fig. 9 Experimental growth rate versus growth temperature

high as $10 \mu\text{m h}^{-1}$ (at high temperatures). This indicates that there is perhaps a way of improvement in term of higher growth rates of epitaxial layers by decreasing further the supersaturation (i.e., increasing the temperature). However, these conditions correspond also to the beginning of strong etching phenomena, both for AlN [47] and sapphire [48]. It is not sure that this area can be reached in high-temperature HVPE, mainly due to HCl by-product formation and H_2 etching.

As supersaturation is essentially dependent on temperature due to the exponential relationship between “AlN vapor pressure” and temperature, a simple way of plotting all our experiments could be to represent directly the experimental growth rate versus the growth temperature, as represented in Fig. 9. This figure allows defining a similar process window such as Fig. 8, showing that low-temperature epitaxial layers can be grown at very low growth rate and that high growth rate epitaxial layers can be reached only at high temperatures, whatever the N/Al ratio. It can be optimistically emphasized from this figure that the maximal growth rate that can be reached at $1,500^\circ\text{C}$ could be as high as $25 \mu\text{m h}^{-1}$ and at $1,600^\circ\text{C}$ could be around $70 \mu\text{m h}^{-1}$, if no etching reactions occur. Growth rates as high as $57 \mu\text{m h}^{-1}$ at $1,450^\circ\text{C}$ and N/Al of 4 have been reported in another apparatus with similar process conditions [49].

3.4 Limitations of the numerical modeling to understand AlN epitaxial growth

Crystal quality is linked to high diffusion length of adatoms and low incorporation rate (so high temperature, low supersaturation). The numerical modeling proposed here does not take into account the surface diffusion mechanisms, essentially due to a lack of data in the literature.

The only striking result of this modeling is that contrary to what is classically stated for III–V epitaxy, the III-compound containing species (AlCl_3 and AlCl_2NH_2 here) have a relatively low apparent sticking coefficient (at most 0.013 for AlCl_3 and 0.056 for AlCl_2NH_2 at 1,500 °C in our modeling). As gas-phase aluminum species seem to have a poor affinity with the growing surface (due to steric hindrance or species stability), their surface diffusion length could be high compared to other III-compound or other aluminum precursors.

During III–V epitaxial growth, the III–V ratio is classically kept to a high value to force a kinetic regime limited by a III-compound. This allows increasing the diffusion length of Al adatoms. This condition is clearly not necessary in the case of AlN epitaxial growth in HVPE conditions where the relatively poorly reactive AlCl_3 precursor is the main gas species for aluminum.

4 Conclusion

This study presents a numerical modeling of AlN growth by high-temperature-HVPE which comprises a relatively limited number of chemical reactions. This modeling was experimentally validated within a broad range of process parameters (temperature, N/Al ratio in gas phase). Moreover, this study permitted the calculation of various local parameters such as the surface site ratio and the local supersaturation during AlN growth. On the basis of numerical results, sets of experiments have been designed to assess the influence of N/Al ratio in the gas phase at constant supersaturation on the growing AlN surface or at constant AlN growth rate.

In one hand, it appears that the N/Al ratio or $[\text{N}(\text{S})/\text{Al}(\text{S})]$ is not of prime importance to explain the occurrence of epitaxial growth of AlN on sapphire. However, it has to be carefully controlled to enhance the crystal quality when epitaxial growth is obtained. It was found that (1) a value of $\text{N}/\text{Al} = 1.5$ in the gas phase is optimal to regrow AlN on AlN templates at high temperature and (2) a value of N/Al of 3 in the gas phase is necessary to grow a low-temperature protective layer. The simulated local conditions do not explain these ratios.

On the other hand, simple plots representing growth rate–supersaturation versus temperature clearly exhibit a process window where epitaxial growth could occur. As expected, high epitaxial growth rates need low supersaturation or high temperatures. Simple extrapolations indicate that the domain of improvement in epitaxial growth rates on sapphire is not so wide, due to the fast decomposition of sapphire and AlN at temperatures above 1,500 °C in hydrogen.

Mass transport simulation and theoretical chemistry were used to design sets of experiments. However, the lack of clear macroscopic relationship (except the well-established supersaturation/quality) between process conditions and crystal quality let us to think that at least another parameter plays a key role. It appears that the chemical stability of the interface AlN/sapphire during the first steps of growth is of prime interest compared to the thickening of the layer which is less sensitive to growth conditions. This primary step is also sensitive to N/Al ratio, but its dependence is still not clear. Use of such modeling for the design of experiments is an interesting tool and has to be pursued. The knowledge of local parameters near the growth surface which are reactor-independent could also be used in the development of new reactor configuration.

References

- Kinoshita T, Hironaka K, Obata T, Nagashima T, Dalmau R, Schlessner R, Moody B, Xie JQ, Inoue S, Kumagai Y, Koukitu A, Sitar Z (2012) *Appl Phys Express* 5:122101
- Balandras S, Reinhardt A, Laude V, Soufyane A, Camou S, Daniau W, Pastureaud T, Steichen W, Lardat R, Solal M, Ventura P (2004) *J Appl Phys* 96:7731–7741
- Piazza G, Felmetger V, Murali P, Olsson RH, Ruby R (2012) *MRS Bull* 37:1051–1061
- Slack GA, McNelly TF (1977) *J Cryst Growth* 42:560–563
- Tian W, Yan WY, Dai JN, Li SL, Tian Y, Hui X, Zhang JB, Fang YY, Wu ZH, Chen CQ (2013) *J Phys D Appl Phys* 46:065303
- Nickel KG, Riedel R, Petzow G (1989) *J Am Ceram Soc* 72(10):1804–1810
- Kumagai Y, Yamane T, Miyaji T, Murakami H, Kangawa Y, Koukitu A (2003) *Phys Status Solidi (c)* 7:2498–2501
- Kumagai Y, Yamane T, Koukitu A (2005) *J Cryst Growth* 281:62–67
- Freitas JA, Culbertson JC, Mastro MA, Kumagai Y, Koukitu A (2012) *J Cryst Growth* 350:33–37
- Nagashima T, Harada M, Yanagi H, Kumagai Y, Koukitu A, Takada K (2007) *J Cryst Growth* 300:42–44
- Eriguchi K, Murakami H, Panyukova U, Kumagai Y, Ohira S, Koukitu A (2007) *J Cryst Growth* 298:332–335
- Eriguchi K, Hiratsuka T, Marukami H, Kumagai Y, Koukitu A (2008) *J Cryst Growth* 310:4016–4019
- Tajima J, Murakami H, Kumagai Y, Takada K, Koukitu A (2009) *J Cryst Growth* 311:2837–2839
- Claudel A, Blanquet E, Chaussende D, Audier M, Pique D, Pons M (2009) *J Cryst Growth* 311:3371–3379
- Balaji M, Claudel A, Fellmann V, Gelard I, Blanquet E, Boichot R, Pierret A, Attal-Tretout B, Crisci A, Coindeau S, Roussel H, Pique D, Baskar K, Pons M, Alloy J (2012) *Compound* 526:103–109
- Claudel A, Blanquet E, Chaussende D, Boichot R, Doisneau B, Berthome G, Crisci A, Mank H, Moisson C, Pique D, Pons M (2011) *J Cryst Growth* 335:17–24
- Allendorf MD, Osterheld TH In: *Proceedings of the electrochemical society*, vol 96-5
- Mc Daniel AH, Allendorf MD (1998) *J Phys Chem A* 102:7804–7812

19. McDaniel AH, Allendorf MD (1997) In: Proceedings of the CVDXIV/EUROCVI 11, vol 97-25. The Electrochemical Society, Pennington, p 40
20. Allendorf MD, Melius CF, Osterheld TH (1996) Mater Res Soc Proc 410:459
21. Miller JA, Bowman CT (1989) Prog Energy Combust Sci 15:287
22. Dollet A, Casaux Y, Chaix G, Dupuy C (2002) Thin Solid Films 406:1–16
23. Swihart MT, Catoire L, Legrand B, Gökalp I, Paillard C (2003) Combust Flame 132:91–101
24. Cai D, Zheng LL, Zhang H, Tassev VL, Bliss VF (2005) J Cryst Growth 276:182–193
25. Cai D, Zheng LL, Zhang H, Tassev VL, Bliss VF (2006) J Cryst Growth 293:136–145
26. Segal AS, Bazarevskiy DS, Bogdanov MV, Yakovlev EV (2009) Phys Status Solidi (c) 6:S329–S332
27. Boichot R, Claudel A, Baccar N, Milet A, Blanquet E, Pons M (2010) Surf Coat Technol 205:1294
28. Kee RJ, Rupley FM, Meeks E, Miller JA Chemkin-III: a FORTRAN chemical kinetics package for the analysis of gas phase chemical and plasma kinetics. Sandia National Laboratories. Livermore, California
29. Bird RB, Stewart WE, Lighfoot EN (2002) Transport phenomena, 2nd edn. Wiley, New York
30. Svehla RA (1962) NASA technical report R-132. NASA-TR-R-132
31. Taylor R, Krishna R (1993) Multicomponent mass transfer. Wiley, New York
32. JANAF Thermochemical tables, 3rd edn. The American Chemical Society (Washington) and the American Institute of Physics (New York) for the National Bureau of Standards, USA
33. <http://www.sandia.gov/HiTempThermo/>
34. Coltrin ME, Kee RJ, Rupley FM (1990) Surface CHEMKIN. Sandia National Laboratories. Livermore, California
35. Blocher JM (1974) J Vac Sci Technol 11(4):680–686
36. Råback P, Nieminen R, Yakimova R, Tuominen M, Janzén E (1997) J Electrochem Soc 144:1024–1027
37. Bloem J, Oei YS, de Moor HHC, Hansen JHL, Giling LJ (1985) J Electron Soc 132(8):1973–1980
38. Hwang NM, Yoon DY (1994) J Mater Sci Lett 13(19):1437–1439
39. Giling LJ, De Moor HHC, Jacobs WPJH, Saaman AA (1986) J Cryst Growth 78(2):303–321
40. Tai C, Shih C-Y (1996) J Cryst Growth 160(1–2):186–189
41. Vahlas C, Hwang NM, Gueroudji L, Maury F (1998) Chem Vap Depos 4(3):96–99
42. <http://www.sgte.org/>
43. Boichot R, Coudurier N, Mercier F, Lay S, Crisci A, Coindeau S, Claudel A, Blanquet E, Pons M (2013) Surf Coat Technol. doi:10.1016/j.surfcoat.2013.08.016
44. Pons M, Boichot R, Coudurier N, Claudel A, Blanquet E, Lay S, Mercier F, Pique D (2013) Surf Coat Technol 230:111–118
45. Claudel A, Blanquet E, Chaussende D, Boichot R, Martin R, Mank H, Crisci A, Doisneau B, Chaudouet P, Coindeau S, Pique D, Pons M (2011) J Electrochem Soc 158(3):H328–H332
46. Kumagai Y, Enatsu Y, Ishizuki M, Kubota Y, Tajima J, Nagashima T, Murakami H, Takada K, Koukitu A (2010) J Cryst Growth 312:2530–2536
47. Claudel A, Blanquet E, Chaussende D, Boichot R, Doisneau B, Berthomé G, Crisci A, Mank H, Moisson C, Pique D, Pons M (2011) J Cryst Growth 335(1):17–24
48. Akiyama K, Araki T, Murakami H, Kumagai Y, Koukitu A (2007) Phys Status Solidi (c) 4(7):2297–2300
49. Nagashima T, Harada M, Yanagi H, Fukuyama H, Kumagai Y, Koukitu A, Takada K (2007) J Cryst Growth 305:355–359